

# Search for correlations between *COBE* DMR and *ROSAT* PSPC All-Sky survey data

Rüdiger Kneissl<sup>1</sup>, Roland Egger<sup>2</sup>, Günther Hasinger<sup>3</sup>, Andrzej M. Sołtan<sup>4</sup>, and Joachim Trümper<sup>2</sup>

<sup>1</sup> Max-Planck-Institut für Astrophysik, Karl-Schwarzschild-Str.1, D-85748 Garching bei München, Germany

<sup>2</sup> Max-Planck-Institut für Extraterrestrische Physik, D-85748 Garching bei München, Germany

<sup>3</sup> Astrophysikalisches Institut, An der Sternwarte 16, D-14482 Potsdam, Germany

<sup>4</sup> Copernicus Astronomical Center, Bartycka 18, 00-716 Warsaw, Poland

Received July 10, accepted October 1, 1996

**Abstract.** Results from a cross-correlation analysis between the COBE DMR 4 year, and ROSAT PSPC All-Sky Survey data are presented. Statistical comparisons between microwave and X-ray maps can probe interesting astrophysical environments and processes, such as the warm interstellar medium, the Sunyaev-Zel'dovich effect in clusters of galaxies or gaseous group halos, X-ray luminous radio sources and the Integrated Sachs-Wolfe or the Rees-Sciama effect. In order to test the diffuse, extragalactic X-ray background as probed by ROSAT, against the COBE DMR large-scale CMB structure, our analysis was performed in most detail in a ROSAT selected region of the sky ( $+40^\circ < b, 70^\circ < l < 250^\circ$ ) in an X-ray energy range with minimal Galactic structure and residual X-ray contamination, and the COBE low noise and least Galactic contribution channels. Comparing to other regions of the sky and neighbouring energies and frequencies, we find indication for a positive Galactic correlation on large scales. This correlation is most prominent in the softest X-ray band and lowest microwave channel, with a  $> 95\%$  confidence level detection against COBE noise and CMB cosmic variance, including the high quadrupole value resulting from the power spectrum fit. The spectral dependences are consistent with Galactic thermal X-ray emission, and Galactic synchrotron radiation or free-free (Bremsstrahlung) emission by the warm interstellar medium in the microwave regime. Removing the quadrupole term on a sky map with a Galactic cutout or related gradients in the selected regions leaves no correlations above a  $1-\sigma$  level on smaller angular scales. We conclude that there is no significant extragalactic correlation on scales for which the combined data are sensitive ( $7^\circ - 40^\circ$ ) and that Galactic correlation is significant only on large angular scales, of the order of the quadrupole. In the context of removing large angular scale gradients we

give results on best fit X-ray dipoles from various ROSAT data and discuss these with respect to the difficulty of finding a cosmological dipole. The lowest correlation upper limits we can place are  $\sim 15\%$  of COBE CMB fluctuations and  $\sim 10\%$  of the ROSAT extragalactic XRB fluctuations. We discuss these results with respect to the possible correlation mechanisms.

**Key words:** galaxies: clusters: general — cosmology: cosmic microwave background — cosmology: observations — cosmology: diffuse radiation — X-rays: general

## 1. Introduction

Astrophysical radiation backgrounds are an important probe in cosmology. The instrument data used in this analysis, taken by the Cosmic Background Explorer's (COBE) Differential Microwave Radiometer (DMR) (Smoot et al. 1990) and the Röntgen Satellite's (ROSAT) (Trümper et al. 1990) Position Sensitive Proportional Counter (PSPC) (Pfeffermann et al. 1986) All-Sky Survey (RASS) have contributed to the improvement of our knowledge of the cosmic microwave (CMB) and the cosmic X-ray background (XRB). The COBE DMR discovered for the first time structure of cosmic origin in the CMB (Smoot et al. 1992). The ROSAT PSPC data helped to resolve a large fraction (more than 75%) of the emissivity of the XRB into point sources with redshifts out to  $z \sim 3$  (Hasinger et al. 1993, Comastri et al. 1995).

As the two experiments probe very different energy regimes ( $T_{CMB} = 2.7$  K,  $T_{1keV} = 10^7$  K, Planck temperatures) and the backgrounds originate at different redshifts ( $z_{CMB} \sim 1000$ ,  $z_{XRB} \sim 0-3$ ) no strong correlations can be expected between the two data sets. However physical processes connecting the microwave and X-ray radiation

Send offprint requests to: R. Kneissl,  
ruk@mpa-garching.mpg.de

and common emitting sources do exist, leaving the possibility for a weak correlation.

Both data sets show the Galactic plane prominently and even at high Galactic latitude Galactic emission is present in the maps (Kogut et al. 1996). Correlation in this case can mean spatial alignment of the emitting regions or common physical processes. Galactic contributions to the microwave radiation in the DMR frequencies are synchrotron radiation in the Galactic magnetic field, dust radiation at 18 K, and Bremsstrahlung from the warm interstellar medium of 8000 K (Bennett et al. 1992). The diffuse Galactic X-ray radiation consists of continuum and line emission from hot plasma of 1 to several million K. Structures are mainly constituted by the emission of nearby supernova remnants and superbubbles in the harder bands ( $\sim 1$  keV) but also from absorption through neutral gas associated with HI clouds in the softer bands ( $\lesssim 0.5$  keV) (Snowden et al. 1995; Egger et al. 1996).

An astrophysical environment directly connecting microwave and X-ray radiation is a hot plasma with high column density along the CMB photon path, as was first noticed by Sunyaev & Zel'dovich (1971) (SZ). In clusters of galaxies, electrons with temperatures of  $\sim 10^8$  K and densities of  $\sim 3 \times 10^{-3}$  cm $^{-3}$  scatter photons of the CMB in the inverse Compton process to higher energies leading to  $y$ -distortions of the spectrum and a decrease in photon number in the Rayleigh-Jeans regime. The same plasma, on the other hand, strongly emits at Bremsstrahlung energies of 10 keV. Although the dependences on electron temperature  $T_e$  and electron density  $n_e$  are different for the temperature decrement,  $\Delta T_{SZ}$ , and the X-ray flux,  $S_X$ , according to the approximate relations

$$\begin{aligned}\Delta T_{SZ} &\propto n_e T_e \\ S_X &\propto n_e^2 T_e^{-\frac{1}{2}}\end{aligned}$$

a strong anticorrelation is present and has been observed in individual clusters (e.g. Birkingshaw et al. 1991).

Recently Suto et al. (1996) suggested a similar effect for a possible plasma halo of the Local Group. As the assumed temperature ( $\sim 1$  keV) and density ( $\sim 10^{-4}$  cm $^{-3}$ ) are lower, the expected effect is smaller than for galaxy clusters, but has a predicted angular structure. In the COBE DMR data this structure could not be found (Banday & Górska 1996). A combination with the ROSAT X-ray template, sensitive in this energy range, further improves the limits, also testing for a non-spherical structure of the halo.

Since the XRB does consist to a large extent of point sources, of which the largest fraction are active galaxies (Hasinger et al. 1993), a considerable number are also radio sources, e.g. radio-loud AGN. Laurent-Muehleisen et al. (1996), for example, find 2,127 sources common to the RASS and the Green Bank 5 GHz radio catalog. Correlation analysis can thus test the fraction and angular scale of correlation at which these populations contribute to the data.

Also, recently Turok & Crittenden (1996) proposed the Integrated Sachs-Wolfe (1967) (ISW) effect in a non-flat cosmological model as a possible source for a correlation between CMB and XRB data. This effect, for the non-linear evolution of a single gravitational potential well, also called Rees-Sciama (1968) effect, introduces anisotropies into the CMB via the change of the potential in time  $\Phi$  along the photon path in the direction  $\mathbf{n}$  between recombination  $\tau_{rec}$  and reception  $\tau_0$  time.

$$\frac{\delta T}{T}(\mathbf{n}) = 2 \int_{\tau_{rec}}^{\tau_0} \dot{\Phi}(\tau, \mathbf{n}(\tau_0 - \tau)) d\tau. \quad (1)$$

They calculated the linear evolutionary effect in detail for different  $\Lambda$ -models, with calculations for an open model added by Kamionkowski (1996), and found the largest contribution at  $z < 2$ . Thus, they suggest the distribution of sources in the unresolved XRB to be a tracer of the potential for the redshift interval of interest. If the redshift distribution and the biasing of the sources is known, then a detected positive correlation can quantify  $\Lambda$ . A summary of all these effects (table 2) and a discussion with respect to the results of the correlation analysis is given in section 5.

A statistical comparison between observations of the CMB and the XRB was first carried out by Boughn & Jähoda (1993) comparing the 19.2 GHz survey with HEAO-1 A2 ( $\sim 10$  keV,  $3^\circ$  resolution), and they found no significant correlation, based on Monte Carlo simulations for noise properties. Bennett et al. (1993) in cross-correlating the 1 year DMR data to HEAO-1 found no significant correlation for  $|b| > 30^\circ$  and with the LMC masked. In the 4 year DMR data analysis by Banday et al. (1996) an expansion in orthogonal functions on a cut sky and a likelihood analysis for the coupling constant between the DMR and HEAO-1 data was used in a simultaneous fit to the CMB power spectrum. Again, no significant correlation was found, when applying a specially designed Galactic cut based on correlations obtained from the DIRBE 140  $\mu$ m map and masking of the LMC. Using the ROSAT PSPC extends previous work to softer X-ray energies, higher angular resolution and better sensitivity.

Additional interest in this analysis arises from the detection of a spatially extended X-ray source around clusters of galaxies found in a correlation analysis by Soltan et al. (1996a) between Abell clusters and the ROSAT diffuse XRB. Correlating to the COBE DMR can constrain a gas halo model for the extended component.

In section 2 we introduce the COBE and ROSAT data sets respectively used for this analysis and explain how they were prepared. In section 3 the correlation method is described, including our error estimation. Section 4 contains the results on various angular scales and their dependences with energy or frequency, and in section 5 we discuss the results in the context of theoretical expectations of possible correlation mechanisms.

## 2. The Data

### 2.1. COBE DMR

The COBE DMR measures the sky differentially in 3 frequency channels (31.5, 53 & 90 GHz). The maps are binned in  $2.6^\circ \times 2.6^\circ$  pixels, which are considerably smaller than the beam width of  $7^\circ$  (FWHM). The CMB signal has an amplitude of  $35 \pm 2 \mu\text{K}$  and the COBE DMR mean sensitivity is  $26 \mu\text{K}$  per resolution element, corresponding to a signal to noise ratio of  $\sim 0.5$  on pixel level. The noise level varies from channel to channel (31A: 248, 31B: 316, 53A: 86, 53B: 101, 90A: 146, 90B: 116; in  $\mu\text{K}$  per pixel). The results of the COBE 4 year data analysis by the COBE team are summarized and referenced in Bennett et al. (1996). We used various maps of the *COBE* DMR data set. The final analysis uses the 4 year data, but consistency tests with the 1 year and 2 year data were performed. From the channels A and B, which are differentially measuring the signal, we constructed inverse noise weighted  $(A+B)/2$  and frequency combined sum maps to minimize the noise.

$$\Delta T_{ij} = \frac{1}{W_{ij}}(w_i \Delta T_i + w_j \Delta T_j) \quad (2)$$

with  $w_* = \sum_* 1/\sigma_*^2$  and  $1/W_{ij} = 1/(w_i + w_j)$ , where  $w_*$  is evaluated on the custom cut sky (Banday et al. 1997), considering the noise level and exposure.

All maps used were converted from antenna to Planck temperatures. The standard frequency combination for our analysis is the 53+90 GHz map, with low noise and little Galactic contribution (Kogut et al. 1996). The individual frequency maps and the linearly combined galaxy reduced maps (cmb & smb) were used for comparison.

### 2.2. ROSAT PSPC All-Sky Survey

The ROSAT satellite covers a large energy range (0.1 – 2 keV) in the soft X-rays. The harder part is divided into 4 bands with maximum responses at the following energies (R4: 0.7 keV, R5: 0.8 keV, R6: 1.1 keV, R7: 1.5 keV). All bands, particularly the neighbouring ones, have considerable overlap with each other of up to 50%, due to the limited spectral resolution of the proportional counters.

The RASS intensity ( $I$ ) and noise ( $\sigma$ ) maps were constructed as

$$I = \frac{Ct - B}{Ex} \quad (3)$$

$$\sigma = \frac{\sqrt{Ct}}{Ex} \quad (4)$$

The abbreviations denote count number of received photons ( $Ct$ ), modeled contamination ( $B$ ) and exposure ( $Ex$ ). The X-ray contamination in ROSAT consists, with varying contribution in the different energy bands, of solar scattered X-rays, “short- and long-term enhancements” and particle background. The noise maps are calculated

according to Poisson statistics due to photon number limitation. The energy band R6 (0.73 – 1.56 keV) is regarded as the best probe for the diffuse cosmological XRB, because the systematic uncertainty induced by foregrounds, such as non-cosmic photons, and contamination by charged particles is minimized. We concentrate our analysis and results to this band, but investigate systematic effects by comparison with the other hard bands. Particularly the R5 band is also low in non-cosmic photons and in contamination by charged particles, but which contains, compared to the R6 band, increased Galactic foreground and can thus hint at a discrimination between the Galactic and the extragalactic signal. In spite of the careful corrections for exposure and elimination of non-cosmic backgrounds (Snowden et al. 1995) the final count rate distribution is not completely free from residual contamination. We therefore tested extensively for correlations induced by exposure or contamination corrections and found no negative effects on the results. Unlike the RASS data described in Snowden et al. (1995), the data set used here has been constructed on a “photon by photon” basis, i.e. the intrinsic resolution is that of the detector ( $\sim 1'$ ). Thus, the sensitivity has been improved by avoiding “crosstalk” from bright sources.

The maps used in our work were binned into  $0.7^\circ \times 0.7^\circ$ , with point sources included, in order to compare to the complete integrated flux. In a second step they were rebinned to COBE DMR pixel size with varying exclusion thresholds for bright sources. The mean intensity of the XRB in the R6 is  $\sim 1.9 \text{ cts s}^{-1}$  per pixel with a fluctuation level of  $\sim 0.17 \text{ cts s}^{-1}$  per pixel and a signal to noise ratio of  $\sim 2$  at COBE DMR pixelization.

Even the high energy R6 band is, in large regions of the sky, dominated by Galactic emission. A field almost free from Galactic structures, which is sufficiently large, was chosen ( $+40^\circ < b, 70^\circ < l < 250^\circ$ ), hereafter called the selected NGP field. This field is the largest simply connected patch of the sky probing primarily the XRB. Properties of the XRB in this field have been studied in a series of papers (Soltan et al. 1996a; Miyaji et al. 1996; Soltan et al. 1996b).

## 3. Correlation Method

### 3.1. Correlation Function

To minimize the Galactic contribution, a patch of the sky which has the highest sensitivity to the diffuse, extragalactic XRB was chosen. Due to the size ( $\sim 8\%$  of the sky) and the peculiar geometry of the patch, a local statistical measure for similarities in structure, the 2-point correlation function, is preferred over global measures such as correlated power spectrum components in e.g. a spherical harmonic expansion. The form of the correlation function

used in this analysis is the Pearson product moment correlation coefficient  $C(\alpha) =$

$$\frac{\langle X_i T_j \rangle_\alpha - \langle X_i \rangle_\alpha \langle T_j \rangle_\alpha}{\sqrt{\langle X_i^2 \rangle_\alpha - \langle X_i \rangle_\alpha^2} \sqrt{\langle T_j^2 \rangle_\alpha - \langle T_j \rangle_\alpha^2}} \quad (5)$$

in an unweighted scheme. Inverse noise variance weighting has also been used and was found to give unchanged results. The correlation coefficient varies between 1 and -1 for correlation and anticorrelation respectively with 0 indicating no correlation. For pixel sizes comparable to the resolution limit, the statistical uncertainty of the measure is  $(1 - C^2(\alpha)) \sqrt{N_{\{ij\}} - 1}$ . The average is taken over all pixel pairs  $\{ij\}$  with separation  $\alpha$  in the patch. The subscript  $\alpha$  denotes that all the terms were evaluated separately for each angle bin. This ensures a correctly weighted normalization even in cases when, due to limited area and boundary effects, the zero-lag field properties are not a fair ensemble average for all angle bins any longer. Note that through our choice of the cross-correlation function, the bins are completely statistically independent, and hence any apparent correlation between the bins is due to the structures in the maps.

To determine the uncertainties, which we assume to be dominated by the DMR noise (section 2) and the cosmic variance of the CMB structure, different techniques were applied. We applied a simple method, which introduces little prejudice (just assumes rotational invariance of the data), to correlate to random samples drawn from the maps by rotation. Since the ROSAT maps are known to contain a strong Galactic, not rotationally invariant contribution on major parts of the sky, in contrast to the COBE maps, which have been investigated and found to be primarily consisting of CMB structures (Kogut et al. 1996), and since the COBE data predominantly introduce the errors, those were rotated around the NPG, and mirror image rotated around the SGP in  $10^\circ$  steps to produce 35 and 36 random samples each. The error estimates induced by this method agree well with our second method using simulations of DMR maps. The CMB structure was taken to be a random Gaussian field on the sky with a power-law ( $Q_{rms-PS} = 15.3 \mu\text{K}$ ,  $n = 1.2$ ) power spectrum (Górski et al. 1996) convolved with the DMR filter function (Kneissl & Smoot 1993). The modes used to construct the map cover a range in multipole index  $\ell = 2-25$ . Our results were compared against  $\sim 1000$  simulations. The DMR noise is given as Gaussian pixel noise distributed according to the coverage.

### 3.2. Spherical Harmonic Fit

Although we use a correlation function analysis and not a power spectrum correlation analysis, it is important to study how the correlation results are influenced by par-

ticularly the low order multipoles. For this we expand the sky maps

$$X(\vartheta, \varphi) = \sum_{\ell=0}^{\infty} \sum_{m=-\ell}^{+\ell} b_{\ell m} Y_{\ell m}(\vartheta, \varphi) \quad (6)$$

into real valued spherical harmonics

$$Y_{\ell m}(\vartheta, \varphi) =$$

$$\sqrt{\frac{2\ell+1}{2\pi}} \sqrt{\frac{(\ell-|m|)!}{(\ell+|m|)!}} P_\ell^{|m|}(\cos \vartheta) \begin{cases} \sin |m| \varphi, & m < 0 \\ \frac{1}{\sqrt{2}}, & = 0 \\ \cos |m| \varphi, & > 0 \end{cases}$$

$$P_\ell^m(x) = (-1)^m (1-x^2)^{-\frac{m}{2}} \frac{d^m}{dx^m} P_\ell(x), \quad m > 0 \quad (7)$$

$$P_\ell(x) = \frac{1}{2^\ell \ell!} \frac{d^\ell}{dx^\ell} (x^2 - 1)^\ell$$

in a simultaneous fit up to multipole order  $\ell_{max}$ , and subtract these multipoles from the maps. A well-known problem (e.g. Bunn et al. 1994) arises in this procedure. The orthogonality relation for the spherical harmonics does not hold in the case of incomplete sky coverage:

$$\int_R Y_{\ell m}(\Omega) Y_{\ell' m'}(\Omega) d\Omega = W_{\ell \ell' m m'}, \quad (8)$$

where  $W_{\ell \ell' m m'} \neq \delta_{\ell \ell'} \delta_{m m'}$  in general, if  $R \subset S_1$ . In our case this leads to the fact that we subtract a function from the sky which can be expressed as a sum of different multipoles. Nevertheless the order of angular scale of variation for this function is similar to the dominant multipole probed. Only in close comparison with theoretical power spectrum estimates is an exact determination of the individual multipole terms of interest. For this we investigated the amount of “cross-talk” between the modes by varying  $\ell_{max}$  to the stability limits of the fit and studying the noticeable changes of the subtracted multipole modes, since the limitation to a range in  $\ell$ -space is the major problem for the fit technique. The changes to the results of our correlation analysis and dipole determination turn out to be insignificant at the present sensitivity level. In the case of fitting a dipole to a field the resulting parameters describe the direction and amplitude of a local gradient and can only be compared for consistency with a whole sky dipole. In the case of the correlation analysis the errors induced by the effect are statistically taken into account by subjecting the simulated data to the same subtraction procedure. We find good agreement between the best fit multipoles and expected amplitudes from the correlation results on the region, or a subset of the region for which the fit is constrained. This, combined with the fact that the correlation function seems to be a fairly unbiased estimator for the amplitude of multipoles (Bunn et al. 1994), at least in the case of a power-law model for the CMB

fluctuations, gives us further confidence in the validity of the method used and we did not see the need to apply more sophisticated methods such as, e.g. constructing orthogonalized functions on parts of the sky (Górski 1994) or utilizing model assumptions in Wiener filtering techniques (Zaroubi et al. 1995), in the present state of the work.

### 3.3. Quantifying Results

For quantifying limits on the strength of the correlation ( $\beta$ ), we use a method which evaluates a likelihood distribution for  $\beta$ , see e.g. Bennett et al. (1993). Assuming that the signal in the *ROSAT* data (X) and the *COBE* data (T) can be written in pixel space, leaving out the index  $i$ , as

$$\begin{aligned} T &= T_{CMB} + T_{noise} + \beta_{T|X} X \\ X &= X_{XRB} + X_{noise} + \beta_{X|T} T \end{aligned} \quad (9)$$

where  $\beta_{T|X}$  and  $\beta_{X|T}$  are the regression coefficients which couple the two maps by regarding one as template for the other. Clearly the *COBE* noise and CMB cosmic variance dominating the temperature distribution are the main source of confusion for the cross-correlation. The Poisson noise in *ROSAT* by photon number limitation is apparently a small confusion term. Shot noise is hard to distinguish from the XRB since we are interested in a possible correlation of *ROSAT* sources. From the results of testing with different source exclusion thresholds, we deduce that shot noise is small after exclusion of a few very strong sources. A probably considerable confusion term for the cross-correlation is chance alignment of the structure in the diffuse XRB, which we denoted by  $X_{XRB}$  (here meaning the uncorrelated part). Due to the complexity of the diffuse XRB, which consists of various types of sources, more so than the CMB, no established model for the fluctuations exists. There is interesting work (e.g. Lahav et al. 1996) to model the extragalactic XRB fluctuations, however, these models have not yet been compared to data and hence are still somewhat uncertain. We believe that overall, the *COBE* noise and CMB cosmic variance correlated with the real structure in the *ROSAT* maps are the dominant confusion terms, and for now, we have not attempted to model the XRB. Forming the correlation functions then yields the relations

$$\begin{aligned} \langle XT \rangle &= \langle XT_{CMB} \rangle + \langle XT_{noise} \rangle + \\ &\quad \beta_{T|X} \langle XX \rangle \\ \langle TX \rangle &= \langle TX_{XRB} \rangle + \langle TX_{noise} \rangle + \\ &\quad \beta_{X|T} \langle TT \rangle \end{aligned} \quad (10)$$

where  $\langle XT_{CMB} \rangle$ ,  $\langle XT_{noise} \rangle$ ,  $\langle TX_{XRB} \rangle$  &  $\langle TX_{noise} \rangle$  are assumed to be zero in the sense of a statistical average. This leads to the approximate relations

$$\begin{aligned} \beta_{T|X} &\sim \langle XT \rangle_{0^\circ} / \langle XX \rangle_{0^\circ} \\ \beta_{X|T} &\sim \langle XT \rangle_{0^\circ} / \langle TT \rangle_{0^\circ} . \end{aligned} \quad (11)$$

For one particular realization this is only true within some error, which may be determined through Monte-Carlo simulations assuming models for  $T_{CMB}$ ,  $T_{noise}$ ,  $X_{XRB}$  and  $X_{noise}$ . We also take account of statistical biasing, which turned out to be small in comparison to the random errors. We assume now that  $T_{CMB}$  and  $T_{noise}$  are the dominant sources of error compared to Poisson noise and random structure in the XRB, and approximate  $\langle T(X_{XRB} + X_{noise}) \rangle$  by  $\langle (T_{CMB} + T_{noise})X \rangle$ . Our method of determining  $\beta_{T|X}$  and the corresponding uncertainty is to minimize

$$\chi^2 = \sum_{kl} (\langle TX \rangle - \beta_{T|X} \langle XX \rangle)_k^T M_{kl}^{-1} (\langle TX \rangle - \beta_{T|X} \langle XX \rangle)_l \quad (12)$$

with  $M_{kl} = \langle X(T_{CMB} + T_{noise}) \rangle_{kl}$  which can be determined from a distribution of realizations of the model. Assuming Gaussian errors, the probability distribution for  $\beta$  can be drawn from the  $\chi^2$ -distribution as

$$P(\beta) d\beta \propto e^{-\frac{1}{2}\chi^2} d\beta. \quad (13)$$

## 4. Results on Various Scales

Since the aim of this analysis is to compare a CMB measurement to the diffuse XRB, some individual very strong X-ray point sources, which could influence even a statistical comparison, are removed from the maps. Furthermore, the influence of different point source exclusion thresholds on the results were studied and found to be mostly insignificant. In a few cases, e.g. MK 421, a BL Lac object at  $z \sim 0.031$ , the removal of the source lead to a decrease of the correlation signal on the DMR beam scale. Comparison with known strong radio point sources showed no significant contribution to DMR (Kogut et al. 1994), so chance alignment seems a likely cause. Nevertheless, systematic comparison between *COBE* data and candidate radio-loud X-ray point sources seems a worthwhile check. The best fit DMR residual dipole, which would introduce substantial correlation of no physical significance, had been removed, in addition to the standard removed dipole.

### 4.1. Selected NGP Field

Correlating the raw data (without excluding source contaminated pixels or subtracting structure) yields a marginally significant positive correlation on large angular scales (figure 1), which appeared to be independent of

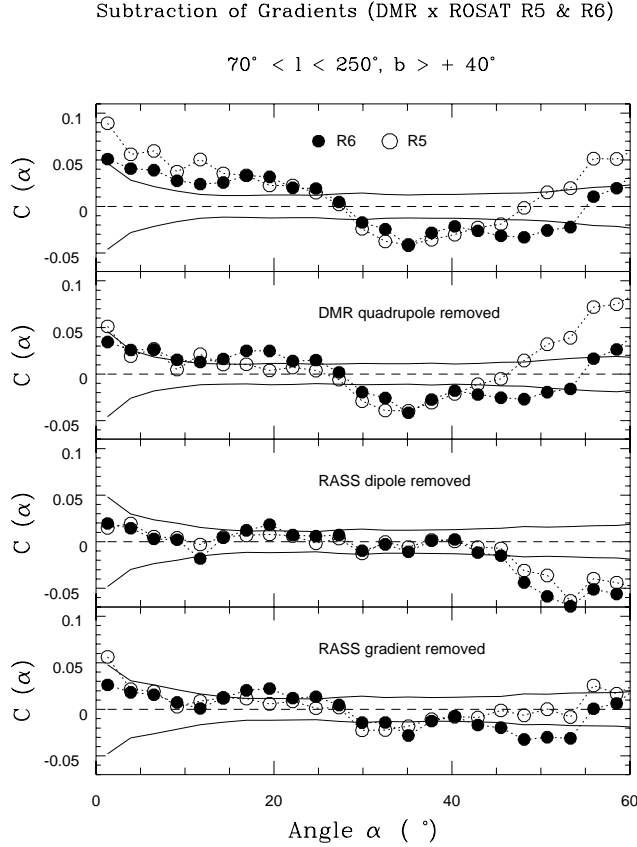


**Fig. 1.** Cross-correlation function between the COBE DMR 53+90 GHz and the ROSAT bands R6 (black) and R5 (white) in the selected NGP field ( $+40^\circ < b < 70^\circ$ ,  $70^\circ < l < 250^\circ$ ). The effect of lowering the zero-lag amplitude by subtracting different multipoles related to a gradient on the field is shown (lowest panel). Subtracted are a best fit quadrupole from the Galactic custom cut DMR map, a best fit dipole which has Galactic signature from the Galactic cut ROSAT map ( $|b| > 20^\circ$ ) and a gradient as a dipole fitted on the field. The two latter both have Galactic signature (table 1). The  $1-\sigma$  error bands are taken from DMR noise + CMB simulations correlated to the ROSAT energy band R6.

the following different procedures that had been applied. Different source exclusion thresholds in the ROSAT maps ranging from  $0.3\text{--}1 \text{ cts s}^{-1}$  were compared. After excluding the strong source MKN 421 with  $5.3 \text{ cts s}^{-1}$  in the R6 energy band, the results were only marginally affected by different thresholds. Different sampling tests were undertaken, also showing stability of the result against small scale features such as point sources and noise. The maps were smoothed on various angular scales including smoothing of the ROSAT maps with the actual DMR beam (Kneissl & Smoot 1993), and Gaussian smoothing of both maps out to  $20^\circ$ , with the effect of smoothing

the correlation function, but not significantly changing the correlated signal.

The energy dependence in X-rays is found to increase from hard to soft energies. The frequency dependence in microwaves is somewhat unclear. There is a clear signal in both the 53 and 90 GHz channels and no signal at 31.5 GHz.

To determine the angular scale of the correlated signal, gradients were removed from the field. This was done in fitting dipoles onto the field in both maps and subtracting them. As a result the signal is reduced below the  $1-\sigma$  level. The multipoles on the sky dominating these gradients turn out to be of low order (figure 1).

The gradient in the ROSAT selected NGP field has similar orientation as the whole map dipole (table 1), the positive pole lying near the Galactic center, and increasing in relative amplitude from hard to soft energies. From this energy dependence we derive spectral properties of the emitter that are in agreement with a  $2 \times 10^6 \text{ K}$  equilibrium plasma, typical for Galactic emission. The energy dependence, however, is not compatible with the X-ray spectrum of the extragalactic XRB (Hasinger et al. 1993).

The gradient in the COBE field is dominated by a quadrupole fitted to the COBE cut sky, a combination of the cosmic and the Galactic quadrupole. In the field, the cosmic quadrupole seems to dominate, which would not be inconsistent with the COBE frequency dependence of the correlated signal. A signal constant with frequency would be expected, but the 31.5 GHz channel could be confused by the increased noise level and Galactic contribution.

Removing the gradients no significant correlation is left, and we can set upper limits of  $4.5 \mu\text{K}$  and  $0.02 \text{ cts s}^{-1}$  per pixel (95 % CL) in the R6 band on a correlation between the CMB and the extragalactic XRB on scales of  $7^\circ - 40^\circ$ .

#### 4.2. Cut Sky

For completeness we present the correlation function on a large fraction of the sky, the DMR Galactic cut sky, although these results are not relevant for a comparison with the extragalactic XRB. We use the DMR cut sky for both data sets, since the most interesting question in this case is that of a correlation to Galactic features in the COBE DMR, which should be largely excluded by the custom cut (Banday et al. 1997), which is a straight  $|b| > 20^\circ$  cut, with additional cutouts for Galactic structures found in correlation to the  $140 \mu\text{m}$  COBE DIRBE map (“flares of obscuration” in Scorpis, Ophiuchus, Taurus and Orion). We additionally experimented with  $|b| > 20^\circ$  and  $30^\circ$ , and found, not surprisingly, a slight, not very significant tendency towards positive correlation with smaller cut angle. To minimize confusion, we subtract before the correlation in the cut sky case, in addition to the best fit DMR dipole, also the best fit ROSAT dipole.

Subtraction of the DMR Quadrupole (DMR 53+90 x ROSAT)

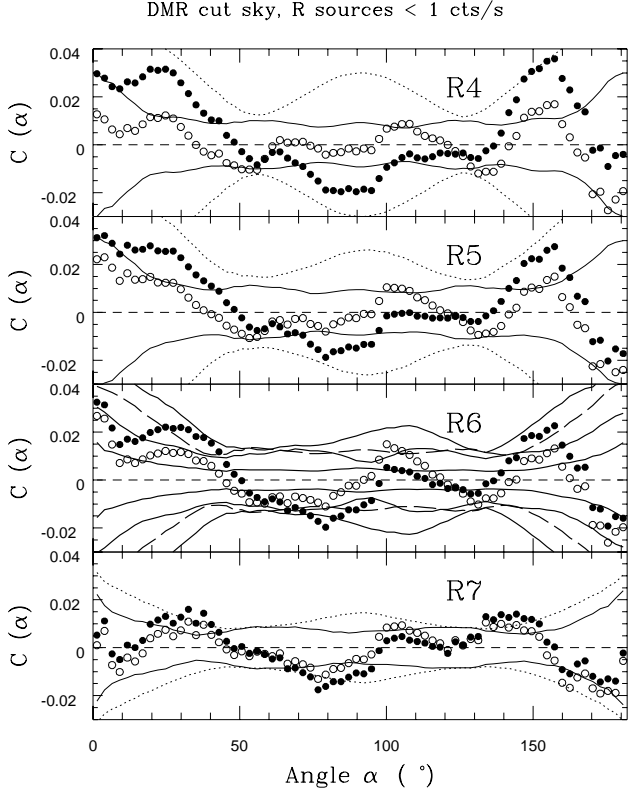


**Fig. 2.** Cross-correlation between DMR 53+90 GHz and different ROSAT energy bands including (black) and excluding (white) the DMR quadrupole. The DMR and ROSAT data are both taken from the same region, i.e. the DMR Galactic cut sky. Apart from the R6 band the narrow (solid line) and wide (dotted line) 1- $\sigma$  error bands are taken from DMR noise and CMB power spectrum simulations excluding and including the variance from the  $Q_{rms-PS} = 15.3 \mu\text{K}$  respectively. In the R6 band panel we demonstrate the 1- $\sigma$  error bands from (with increasing amplitude at zero-lag): DMR noise only, noise + CMB ( $\ell > 2$ ), noise + CMB ( $\ell > 2$ ) +  $Q_{rms}$  ( $= 6 \mu\text{K}$ ) (dashed line) and noise + CMB ( $\ell > 1$ ). There is no significant correlation, but a trend of increasing positive quadrupole correlation towards softer X-ray energy bands with about 68 % CL at R4 against the cosmic variance of  $Q_{rms-PS} = 15.3 \mu\text{K}$ . The small excess in correlation on scales out to  $10^\circ$  most prominent in DMR x R6 has been found to be partly due to the LMC.

The corresponding ROSAT sky is largely dominated by strong Galactic features such as, e.g. the Loop I with the prominent North Polar Spur, or the Eridanus enhancement, which are claimed not to be found in the DMR maps (Kogut et al. 1996) and therefore are sources of confusion. The limits we get confirm this view. The limits on the contribution of ROSAT to COBE are stronger compared to the ones derived on the selected NGP field, but this has to

Subtraction of the DMR Quadrupole (DMR x R5)

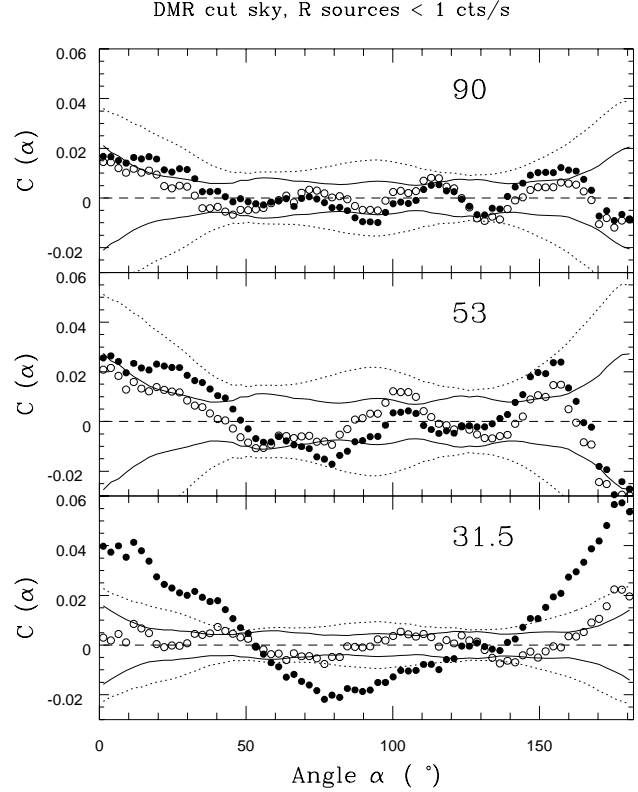


**Fig. 3.** Cross-correlation between ROSAT R5 and the individual DMR frequency channels (GHz) including (black) and excluding (white) the DMR quadrupoles. The DMR and ROSAT data are both taken from the same region, i.e. the DMR Galactic cut sky. The 1- $\sigma$  error bands are taken from DMR noise and CMB simulations including and excluding  $Q_{rms-PS}$  respectively. There is a trend of increasing quadrupole correlation towards lower DMR frequencies with a significant ( $> 95\%$  CL) detection at 31.5 GHz.

be taken with caution, since ROSAT is by a factor of  $\sim 2$  less constrained, due to increased uncorrelated (Galactic) structure in ROSAT.

In figure 2 we find the DMR quadrupole to be positively correlated to the ROSAT R4-6 templates. Here the outer 1- $\sigma$  error bands demonstrate the inclusion of the  $Q_{rms-PS} = 15.3 \mu\text{K}$  quadrupole. We stress here the fact that the huge cosmic variance of this term ( $\sim 68\%$ ) introduces a large error, which is problematic, as the actually measured, uncorrected DMR  $Q_{rms}$  is considerably smaller ( $15.6 \pm 5.4 \mu\text{K}$  [31.5 GHz],  $4.4 \pm 3.3 \mu\text{K}$  [53 GHz],  $0.0 \pm 3.0 \mu\text{K}$  [90 GHz]), because of an apparently anti-correlated alignment of the CMB quadrupole ( $10.7 \pm 3.6$ (random)  $\pm 7.1$ (systematic)  $\mu\text{K}$ ) with the Galactic quadrupole (Kogut et al. 1996). For the energy dependence of the effect, we find agreement with a thermal  $2 \times 10^6 \text{ K}$  spectrum and dis-

agreement with an extragalactic spectrum (a power-law with a photon index  $\Gamma \approx -2$ ).

Comparing the *ROSAT* R5 band to the different DMR frequencies (figure 3) we find a significant positive correlation ( $> 95\%$  CL) at 31.5 GHz due to a quadrupole term ( $Q_{rms}^{COBE} = 10.3 \pm 4 \mu\text{K}$ ,  $Q_{rms}^{ROSAT} = 0.38 \pm 0.15 \text{ cts s}^{-1}$  per pixel). At the other frequencies a correlation due to the quadrupole is also positive, but not significant compared with the full CMB spectrum including the quadrupole. Investigating the spectral dependence we find the spectral index  $\beta$ ,  $T_{antenna} \propto \nu^\beta$ , within  $1\sigma$  to be consistent with  $\beta_{ff} \sim -2.1$  and  $\beta_{synchrotron} \sim -2.8$ .

When subtracting the best fit quadrupole, there is in no case any significant correlation left in the data. The limits are in the case of DMR 53+90 x *ROSAT* R6 on a  $30^\circ$  cut sky  $2.3 \mu\text{K}$  and  $0.037 \text{ cts s}^{-1}$  per pixel (95 % CL).

From the systematics of the quadrupole correlation, we conclude that a correlation between Galactic quadrupoles in *ROSAT* and *COBE* seems likely, but which however, apart from the *COBE* DMR 31.5 GHz channels, can not be shown with sufficient significance against the cosmic variance of a quadrupole consistent with the CMB spectrum. We see this result in agreement with the existence of a Galactic DMR quadrupole (Bennett et al. 1992; Kogut et al. 1996).

#### 4.3. Dipole

The *COBE* dipole is the well known Doppler dipole due to the sun's motion with respect to the CMB rest frame. Any other residual dipole is an inseparable combination of imperfect Doppler dipole subtraction, Galactic dipole and CMB dipole. Thus a best fit dipole has to be removed from the maps, because the induced correlation has no physical interpretation and thus confuses the results. Still the best fit dipoles in *ROSAT* can be determined and simply compared to amplitude and orientation of e.g. the DMR Doppler dipole, an expected Galactic dipole, etc.

The dominant part of the correlated signal on the selected NPG field can be explained by a Galactic gradient in *ROSAT*. Comparing orientation and amplitude of this gradient expressed as a dipole on the sky, to dipoles fitted to other regions (table 1), we find it to lie in the general direction of the Galactic center and North Polar Spur region and to have an amplitude of the dipole component towards the Galactic center ( $\tilde{b}_{11}$ ) which significantly increases towards softer X-rays, consistent with a Galactic energy spectrum. An increase in Galactic latitude towards harder X-rays in the selected NPG field, although also preferred by fitting in the SGP field, has to be attributed to local Galactic phenomena, since it is not supported by a more global, joint fit to both fields combined. The  $\chi^2/\text{degrees of freedom (dof)}$  indicates that the gradients / dipoles are clearly not the dominant structures, but they are fairly well defined in terms of the formal fit errors and insensitive to point source contributions (compare panels 3

and 4 of table 1). For the determination of an extragalactic global dipole, systematic errors induced by Galactic features appear to be the overwhelming source of confusion. The dipole fits presented here can be compared to work by Freyberg et al. (1996), who investigated the *ROSAT* data with regards to a possible Galactic X-ray halo.

## 5. Discussion

### 5.1. Dipole

Comparison of the dipole components is of interest, because the firm detection of a cosmological X-ray dipole can either give confirmation to the velocity interpretation of the CMB dipole, or probe the distribution of matter on intermediate scales (100 - 1000  $\text{h}^{-1} \text{ Mpc}$ ) and redshifts ( $z < 5$ ). The velocity dipole amplitude can be calculated from the Compton-Getting effect (Compton & Getting 1935) incorporating the relativistic effects of aberration and spectral shift to

$$\frac{I_{CG}}{I} = (2 + \Gamma) \frac{v}{c} \cos \Theta. \quad (14)$$

The photon index ( $n(E) \propto E^{-\Gamma}$ ) for the extragalactic XRB in the *ROSAT* energy bands is  $\Gamma_{ROSAT} = 2.0 \pm 0.1$  (Hasinger et al. 1993) and the sun's velocity with respect to the CMB has been measured in the *COBE* DMR to be  $v = 369.0 \pm 2.5 \text{ km/s}$  in the direction  $(\ell, b) = (264^\circ.31 \pm 0^\circ.17, +48^\circ.05 \pm 0^\circ.10)$  (Lineweaver et al. 1996). With these numbers, the expected dipole rms amplitude, expressed as a percentage of the monopole term, is  $D_{CG} = 0.08$ . This is more than an order of magnitude lower than our typically measured dipole amplitudes (cf. to the last column of table 1, which gives the observed values expressed in the same manner). A dipole resulting from the distribution of matter is theoretically less well determined, but is assumed to have comparable amplitude to the Compton-Getting dipole (Lahav et al. 1996). Thus, the expected extragalactic dipoles have amplitudes lower than our observed values.

Since we know from the energy dependence and orientation the Galactic origin of the fitted dipoles, our conclusion is that the *ROSAT* data over the energy range from 0.5 – 2 keV are, in major regions of the sky, strongly dominated by a dipolar Galactic structure and a considerable effort would be needed to separate out an extragalactic dipole, if existent in the data.

### 5.2. Galactic Quadrupole

Strong Galactic correlation between the data should not be expected. A spatial correlation between regions of radio free-free (Bremsstrahlung) emission and HII regions ( $\text{H}_\alpha$ ) is plausible. However, it is still unclear if the X-ray signature of HII regions is dominated by emission from associated hot gas or absorption by associated neutral gas.

NGP 70–250 src < 0.45	dof	$\chi^2/\text{dof}$	$b_{00}$	$\tilde{b}_{1-1}$	$\tilde{b}_{10}$	$\tilde{b}_{11}$	$\ell^{II}$	$b^{II}$	D
R4	548	5.3	217 $\pm$ 4	1.1 $\pm$ 0.3	0.6 $\pm$ 1.2	27.7 $\pm$ 0.8	2.3	1.9	7.8
R5	548	4.4	227 $\pm$ 4	-0.6 $\pm$ 0.3	5.3 $\pm$ 1.1	14.2 $\pm$ 0.6	357.6	27.8	4.3
R6	548	5.4	272 $\pm$ 4	-0.5 $\pm$ 0.3	3.3 $\pm$ 1.0	5.3 $\pm$ 0.5	354.7	40.8	1.8
R7	548	3.4	146 $\pm$ 4	-0.9 $\pm$ 0.5	6.4 $\pm$ 1.7	1.0 $\pm$ 0.8	316.4	81.5	1.8
SGP 70–250 src < 0.45									
R4	548	10.8	221 $\pm$ 5	-6.3 $\pm$ 0.4	12.8 $\pm$ 1.3	2.9 $\pm$ 0.7	294.6	69.0	4.1
R5	548	8.4	249 $\pm$ 5	-3.1 $\pm$ 0.3	9.4 $\pm$ 1.2	-0.8 $\pm$ 0.6	255.3	76.5	2.8
R6	548	6.1	305 $\pm$ 5	-2.5 $\pm$ 0.3	6.6 $\pm$ 1.1	2.8 $\pm$ 0.5	318.1	68.3	2.1
R7	548	3.0	208 $\pm$ 5	-2.7 $\pm$ 0.4	13.0 $\pm$ 1.5	7.1 $\pm$ 0.7	339.0	67.5	4.2
N+SGP 70–250 src < 0.45									
R4	1100	10.2	200 $\pm$ 0.6	-1.3 $\pm$ 0.2	3.0 $\pm$ 0.1	17.3 $\pm$ 0.4	355.7	14.0	5.0
R5	1100	7.2	231 $\pm$ 0.6	-1.4 $\pm$ 0.2	2.2 $\pm$ 0.1	7.6 $\pm$ 0.4	349.4	21.8	2.3
R6	1100	5.8	281 $\pm$ 0.6	-1.2 $\pm$ 0.2	1.0 $\pm$ 0.1	4.1 $\pm$ 0.3	343.5	18.2	1.2
R7	1100	3.3	162 $\pm$ 0.6	-1.6 $\pm$ 0.3	-0.4 $\pm$ 0.1	3.1 $\pm$ 0.5	332.6	-8.7	1.0
N+SGP 70–250 src < 1									
R4	1100	10.4	201 $\pm$ 0.6	-1.4 $\pm$ 0.2	3.1 $\pm$ 0.1	17.5 $\pm$ 0.4	355.4	14.0	5.0
R5	1100	8.4	232 $\pm$ 0.6	-1.5 $\pm$ 0.2	2.2 $\pm$ 0.1	8.0 $\pm$ 0.4	349.4	21.0	2.4
R6	1100	7.3	282 $\pm$ 0.6	-1.1 $\pm$ 0.2	1.0 $\pm$ 0.1	3.9 $\pm$ 0.3	344.9	19.6	1.2
R7	1100	3.5	163 $\pm$ 0.5	-1.7 $\pm$ 0.3	-0.4 $\pm$ 0.1	3.3 $\pm$ 0.5	333.4	-8.2	1.1
cut sky ( $ b  > 20$ ) src < 1									
R4	4012	36.8	231.0 $\pm$ 0.2	-4.3 $\pm$ 0.1	5.9 $\pm$ 0.1	30.0 $\pm$ 0.1	351.8	15.5	8.7
R5	4012	54.3	275.7 $\pm$ 0.2	-5.3 $\pm$ 0.1	4.2 $\pm$ 0.1	26.4 $\pm$ 0.1	348.7	12.4	7.7
R6	4012	34.8	315.9 $\pm$ 0.2	-4.2 $\pm$ 0.1	2.5 $\pm$ 0.1	16.9 $\pm$ 0.1	346.1	11.6	5.0
R7	4012	7.1	169.3 $\pm$ 0.2	-3.5 $\pm$ 0.1	0.6 $\pm$ 0.1	6.0 $\pm$ 0.1	329.4	7.2	2.0

**Table 1.** Dipole fits to various subsets of the *ROSAT* PSPC All-Sky Survey data. The fields NGP ( $b > +40^\circ$ ) and SGP ( $b < -40^\circ$ ) are in the longitude ranges indicated. The source exclusion thresholds (src) are in  $\text{cts s}^{-1}$ .  $b_{\ell m}$  are the coefficients of the real valued spherical harmonics, whereas  $\tilde{b}_{1m}$  is  $100 \times b_{1m} / b_{00}$ , the dipole coefficients in percentage of the monopole term. ( $\ell^{II}$ ,  $b^{II}$ ) gives the best fit position for the positive pole in Galactic coordinates and  $D^2 = 1/(4\pi) \sum_{m=-1}^1 \tilde{b}_{1m}^2$  is the amplitude. Although we show the (small) fit errors on the  $\tilde{b}_{1m}$  resulting from *ROSAT* noise only, we do not translate them into the coordinate values as we see the results dominated by systematic errors. For details see text.

Only in the first case would a positive correlation be expected.

Supernova remnants are prominent Galactic features in the soft X-rays, and enrich the Galactic medium with compressed magnetic fields that are responsible for synchrotron emission also at microwave frequencies. However, under the usual assumptions regarding the spectral behaviour of these synchrotron sources, a strong contribution at COBE frequencies is not to be expected. This is in agreement with the lack of correlation (Kogut et al. 1996) between COBE DMR and the template for synchrotron radiation, the 408 MHz map (Haslam et al. 1982). The North Polar Spur, which traces the rim of the nearby

superbubble Loop I (e.g. Egger et al. 1996), is however the most prominent synchrotron source and one positive pole of the correlated quadrupole lies in the corresponding direction. The amplitude of the correlated signal in the COBE DMR is not incompatible with the signal expected from this object in the microwave band, given the uncertainty in the spectral index. Since the North Polar Spur is also known as a very bright X-ray source it is possible that this feature is associated with the correlation.

Although the contribution of the correlated quadrupole to the CMB channels in the DMR is comparatively small, it will be interesting to investigate the meaning of the detection at 31.5 GHz

EFFECT / SOURCE	SIGN	ANGULAR SCALE	FREQU. DEP. microwave	ENERGY DEP. X-ray	AUTHOR
<b>Galaxy</b> geometrical ?	+(−) X-abs.	large	$\beta_{synch, ff, dust} \approx \{-2.8, -2.1, 1.5\}$	thermal 0.3 keV	
<b>SZ thermal</b> (clusters / super- )	− (Rayleigh–Jeans)	( $< 10^\circ$ clust./ $\lesssim 5^\circ$ c-corr.)	y - distortion	thermal 10 keV	
<b>SZ thermal</b> local group halo	− (Rayleigh–Jeans)	large	y - distortion	thermal 1 keV	[1]
X-ray/radio point sources	+	small	flat, $\alpha < 0.5$ (10 – 100 GHz)	$\Gamma \approx 2.0 \pm 0.1$ $I = I_0(E/E_0)^{-\Gamma}$	[2,3,4]
<b>ISW / RS</b> in $\Lambda$ / open universe	+	large $\ell \approx 10$	Planck	$\Gamma \approx 2.0 \pm 0.1$ $I = I_0(E/E_0)^{-\Gamma}$	[5,6]

**Table 2.** Overview of different effects introducing possible correlations between microwave and X-ray data. Authors: [1] Suto et al. 1996, [2] Franceschini et al. 1989, [3] Franceschini 1995, [4] Laurent-Muehleisen et al. 1996, [5] Crittenden & Turok 1996, [6] Kamionkowski 1996.

further, by comparison with the Galactic synchrotron radiation template and the template for Bremsstrahlung and dust radiation (which is the COBE DIRBE 140  $\mu$ m map). These topics will be addressed in a forthcoming paper. By doing this, a separation between synchrotron radiation and Bremsstrahlung might be possible. The answer to the question of whether a physical effect or purely geometrical alignment is responsible for the correlations could be decided.

### 5.3. Derivation of Limits

On the selected NGP field some indication of a positive correlation of large angular scale was found. Since the correlated gradient in ROSAT is of Galactic origin, chance alignment with the COBE CMB quadrupole, and possibly some spatial alignment with the COBE Galactic quadrupole (see section 5.2) turns out to be the cause, and not an extragalactic correlation. After subtracting the dipole and quadrupole terms from a Galactic cut sky, or related large angular scale gradients from the selected NGP field, no significant correlations are found in the data. This will enables us to set limits on a number of possible mechanisms for introducing correlations as described in the introduction and summarized in table 2. We note here, that all our findings are in no conflict with the

standard cosmological interpretation of the COBE DMR measurements.

The large-scale, correlated feature we are seeing, the presumable Galactic quadrupole, cannot originate from the SZ effect, as would be the case for the Local Group halo, since the observed correlation is positive. So at the quoted sensitivity, no Local Group halo is found. By making use of the specific halo template the sensitivity might be improved.

From the temperature limits on the selected NGP area we can infer limits on the Comptonization parameter  $y$  on scales of  $7^\circ$ – $40^\circ$  from distortions in the Rayleigh–Jeans regime

$$\delta T/T = -2\delta y \quad (15)$$

and find  $\delta y < 8 \times 10^{-7}$ . More specific constrains will be derived by combining the DMR and ROSAT limits with model assumptions about the distribution of the gas and its properties. For the gas halo model adopted by Soltan et al. (1996a) as one explanation for the extended correlated X-ray emission around clusters of galaxies, we can limit the assumed temperature of smoothly distributed gas to less than 2 keV (95 % CL). Miyaji et al. (1996), when correlating ROSAT to HEAO, found excess fluctuations at ROSAT energies in comparison to predictions from the population synthesis model by Comastri et al.

(1995). These fluctuations can be explained with excess emission by the gas halo model only when a temperature of at least 2 keV is assumed. Combined with our limits, this leaves a very narrow, possible temperature range for the gas.

Also the combined contribution to the microwave and X-ray fluxes of a population of radio-loud AGNs can be limited, taking into account that the sensitivity for the correlated locations is limited to the zero-lag convolved with the DMR beam.

No indications for a correlation through the ISW have been seen, which should dominate in the high DMR frequencies and hard X-rays. In this case, where we are interested in correlations between the CMB and the extragalactic XRB at a range of scales from a few degrees up to the quadrupole, another search strategy could be adopted, correlating the selected NGP field to the DMR cut sky with the effect of slightly improving the sensitivity on scales of the size of the field, as tests have shown, and quantifying the sensitivity on scales above. Since we do not know how well the fluctuations in the ROSAT XRB trace the projected gravitational potential, although rough assumptions can be made from the properties of the resolved sources (Comastri et al. 1995), we do not give any limits on a  $\Lambda$ -universe in this analysis.

Comparing the limits derived on the selected NGP field and on the  $30^\circ$  cut sky, we find them to differ only marginally. Two effects, reduction of  $\sqrt{N}$ -noise in COBE and increase of predominantly uncorrelated Galactic structure in ROSAT, when going from the smaller to the larger area, can be seen. For comparison with the extragalactic, diffuse XRB the limits from the selected NGP field are preferred.

We qualitatively discussed how the limits we found constrain possible correlation mechanisms. A more quantitative study should make use of specific predictions by each individual effect for e.g. frequency and energy dependence, angular scale, spatial orientation etc. which could result in stronger constraints. This analysis is in progress and will be presented in a future publication.

On the observational side, great improvements for this kind of analysis can be expected from future satellite experiments such as the CMB missions MAP and COBRAS/SAMBA (Bersanelli et al. 1996), compared to high resolution X-ray observations such as XMM and AXAF, and the hard X-ray survey ABRIXAS (Friedrich et al. 1996). In terms of statistical analysis a comparison between COBRAS/SAMBA and ABRIXAS appears most promising, since ABRIXAS will be the most sensitive all-sky X-ray survey (0.3–10 keV) and COBRAS/SAMBA will be the CMB mission with highest angular resolution and best frequency coverage, enabling a separation between different frequency dependences such as Planck spectrum,  $y$ -distortions and radio source spectra to be achieved.

*Acknowledgements.* RK is grateful to his supervisor G. Börner and thanks A.J. Banday, C.H. Lineweaver, S.D.M. White and the referee, O. Lahav, for helpful discussions and suggestions. The *ROSAT* project has been supported by the Bundesministerium für Bildung, Wissenschaft, Forschung und Technologie (BMBF/DARA) and by the Max-Planck-Society. The COBE datasets were developed by the NASA Goddard Space Flight Center under the guidance of the COBE Science Working Group and were provided by the NSSDC.

## References

Banday A.J., Górski K.M., Bennett C.L., et al., 1996, ApJ 468, L85  
 Banday A.J., Górski K.M., Bennett C.L., et al., 1997, ApJ in press, *astro-ph/9601065*  
 Banday A.J., Górski K.M., 1996, MNRAS p in press, *astro-ph/9609018*  
 Bennett C.L., Smoot G.F., Hinshaw G., et al., 1992, ApJ 396, L7  
 Bennett C.L., Hinshaw G., Banday A., et al., 1993, ApJ 414, L77  
 Bennett C.L., Banday A.J., Górski, K.M., et al., ApJ 464, L1  
 Bersanelli M., Bouchet F.R., Efstathiou G., et al., 1996, COBRAS/SAMBA, esa report D/SCI(96)3  
 Birkinshaw M., Hughes J.P., Arnaud, K.A., 1991, ApJ 379, 466  
 Boughn S.P., Jahoda K., 1993, ApJ 412, L1  
 Bunn E., Hoffman Y., Silk J., 1994, ApJ 425, 359  
 Comastri A., Setti G., Zamorani G., Hasinger G., 1995, A&A 296, 1  
 Compton, A., Getting I., 1935, Phys Rev 47, 817  
 Crittenden R.G., Turok N., 1996, Phys Rev Lett 76, 575  
 Egger R.J., Freyberg M.J., Morfill G.E., 1996, Space Sci. Rev. 75, 511  
 Franceschini A., Toffolatti L., Danese L., De Zotti G., 1989, ApJ 344, 35  
 Franceschini A., 1995, personal remark  
 Freyberg M.J., et al., 1996, A&A to be submitted  
 Friedrich P., Hasinger G., Richter G., et al., 1996, in *Proceedings of the International Conference on X-ray Astronomy and Astrophysics, "Röntgenstrahlung from the Universe"* p. 681, eds Zimmermann H.U., Trümper J.E. & Yorke H., MPE Report 263  
 Górski K.M., 1994, ApJ 430, L85  
 Górski K.M., Banday A.J., Bennett C.L., et al., 1996, ApJ 464, L11  
 Hasinger G., Burg R., Giacconi R., et al., 1993, A&A 275, 1  
 Haslam C.G.T., Stoffel H., Salter C.J., Wilson W.E., 1982, A&AS 47, 1  
 Kamionkowski M., 1996, Phys Rev D 54, 4169  
 Kneissl R., Smoot G.F., 1993, COBE Note 5053  
 Kogut A., Banday A.J., Bennett C.L., et al., 1994, ApJ 433, 435  
 Kogut A., Banday A.J., Bennett C.L., et al., 1996, ApJ 464, L5  
 Lahav O., Piran T., Treyer M.A., 1996, MNRAS in press  
 Laurent-Muehleisen S.A., Kollgaard R.I., Ryan P.J., et al., 1996, A&AS, in press, *astro-ph/9607058*  
 Lineweaver C.H., Tenorio L., Smoot G.F., et al., 1996, ApJ 470, 38

Miyaji T., Hasinger G., Egger R., Trümper J., Freyberg M.J., 1996, A&A 312, 1

Pfeffermann E., Briel U.G., Hippmann H., et al., 1987, Proc. SPIE 733, 519

Rees M.J., Sciama D.W., 1968, Nature 217, 511

Sachs R.K., Wolfe A.M., 1967, ApJ 147, (1)73

Smoot G.F., Bennett C., Weber R., et al., 1990, ApJ 360, 685

Smoot G.F., Bennett C.L., Kogut A., et al., 1992, ApJ 396, L1

Snowden S.L., Freyberg M.J., Plucinsky P.P., et al., 1995, ApJ 454, 643

Sołtan A.M., Hasinger G., Egger R., Snowden S., Trümper J., 1996a, A&A 305, 17

Sołtan A.M., Hasinger G., Egger R., Snowden S., Trümper J., 1996b, A&A accepted, *astro-ph/9609131*

Sunyaev R.A., Zel'dovich Ya., 1972, Comments Astrophys. Space Phys. 4, 173

Suto Y., Makishima K., Ishisaki Y., Ogasaka Y., 1996, ApJ 461, L33

Trümper J., 1983, Adv. Space Res. 4, (4)241

Zaroubi S., Hoffman Y., Fisher K.B., Lahav O., 1995, ApJ 449, 446